Coherent high frequency instabilities of detonations

Leung C.,[a] Radulescu M.I.,[a] Sharpe G.J.[b]

[a] Department of Mechanical Engineering, University of Ottawa
Ottawa, Canada

[b] School of Mechanical Engineering, University of Leeds
Leeds, UK

1 Introduction

Typically, detonations are highly sensitive to flow perturbations and tend to be unstable. Two main modes of instability have previously been observed. In multiple dimensions, the instability gives rise to complex cellular structures. In one-dimension, the instability manifests itself as a pulsating instability. An understanding of the pulsating mode of instability is an important first step to analyzing the complex multi-dimensional cellular instability. A large body of work, both numerical and analytical, have been devoted to furthering our understanding of the pulsating instability [1–4]. However, despite the numerous insights gained from previous studies, the underlying mechanisms governing the pulsating instabilities remain unclear.

The objective of this work is to study the mechanisms governing the one-dimensional pulsating detonation instability. This work is a numerical study utilizing a simplified two-step chain branching model [5,6]. The mechanisms of pulsations are studied through the reconstruction of the families of characteristics, which give the trajectories of pressure waves and particle paths on an $x-t$ diagram. The characteristics allow us to track and examine the interactions between the pressure waves and particle paths within the detonation structure. An extended version of the present abstract has appeared elsewhere [7].

2 Mathematical model

The motion of the fluid was modelled by the reactive Euler equations:

$$\frac{D\tilde{\rho}}{D\tilde{t}}+\tilde{\rho}\frac{\partial\tilde{u}}{\partial\tilde{x}}=0,\ \frac{D\tilde{u}}{D\tilde{t}}+\frac{1}{\tilde{\rho}}\frac{\partial\tilde{p}}{\partial\tilde{x}}=0,\ \frac{D(\tilde{e}-\lambda_r\tilde{Q})}{D\tilde{t}}+\tilde{p}\frac{D}{D\tilde{t}}(\frac{1}{\tilde{\rho}})=0 \tag{1}$$

with the perfect gas assumption:

$$\tilde{e}=\frac{1}{\gamma-1}\frac{\tilde{p}}{\tilde{\rho}},\ \tilde{c}=\sqrt{\frac{\gamma\tilde{p}}{\tilde{\rho}}} \tag{2}$$

The variables have their usual meaning: $\tilde{\rho}$ is the density, $\tilde{p}$ the pressure, $\tilde{u}$ the velocity, $\tilde{x}$ the space coordinate, $\tilde{t}$ the time coordinate, $\tilde{e}$ the internal energy of the material, $\tilde{c}$ the sound speed, γ the ratio of specific heats, $\tilde{Q}$ the total chemical energy available in the mixture and λ_r the fraction of residual energy available in the mixture. The

Correspondence to: matei@uottawa.ca

tildes denote dimensional values. The two chemical rate laws governing the reaction rates in the two-step model are:

$$\frac{D\lambda_i}{D\tilde{t}} = -H(\lambda_i)K_i exp(-\frac{\tilde{E}a}{\tilde{R}\tilde{T}}) \tag{3}$$

$$\frac{D\lambda_r}{D\tilde{t}} = (1 - H(\lambda_i))K_r(1 - \lambda_r)^\nu \tag{4}$$

$H(\beta)$ is the usual Heaviside function. $\tilde{T}$ is the temperature. λ_i and λ_r are the reaction progress variables for the induction and reaction zones respectively, initially taking values of 1 and 0 in the quiescent mixture. K_i is a scaling constant adjusted to ensure an induction length of unity. ν is the reaction order, and K_r is a reaction rate constant that controls the time scale of heat release. A detailed description of the two-step model can be found in the work of Short and Sharpe [5].

In this work, the variables have been non-dimensionalized by the post-shock density and pressure of the steady detonation profiles, and the length has been scaled by the induction zone length. The scalings are:

$$\rho = \frac{\tilde{\rho}}{\tilde{\rho}_s}, p = \frac{\tilde{p}}{\tilde{p}_s}, T = \frac{\tilde{T}}{\tilde{T}_s}, u = \frac{\tilde{u}}{\sqrt{\tilde{R}\tilde{T}_s}}, Ea = \frac{\tilde{E}a}{\tilde{R}\tilde{T}_s}, Q = \frac{\tilde{Q}}{\tilde{R}\tilde{T}_s}, x = \frac{\tilde{x}}{\tilde{\Delta}_i} \tag{5}$$

where the s subscript denotes the post-shock state in the ZND profile.

3 Numerical methodology

The numerical study was performed using the AMRITA system developed by Quirk [8]. The reactive Euler equations were solved in the lab frame using a Roe solver. AMRITA uses a tiered grid system, $G = (G_0, G_1, ..., G_{lmax})$ where the subgrid G_i has a mesh spacing of $1/2^i$. The base grid, G_0, covers the entire domain while the finer subgrids are used in areas that require higher resolution.

In compressible flows, pressure waves travel at the local sound speed and are convected by the flow. This gives two families of characteristic curves called the C+ and C- characteristics. The C- represent the trajectories of pressure waves travelling toward the rear, and the C+ represent the trajectories of pressure waves travelling toward the front; the positive x direction in our case is taken in the direction of detonation propagation. The third family of characteristics, C0, represent the path of a fluid particle. The C-, C+ and C0 are represented, respectively, by:

$$\frac{dx}{dt} = u - c, \frac{dx}{dt} = u + c, \frac{dx}{dt} = u \tag{6}$$

At the beginning of the simulations, three sets of characteristics were generated. At each time step, a linear interpolation was used to find $u - c, u + c$, and u at each point for each characteristic. Eqs. (6) were then integrated to update the location of the characteristic at the next time step. The integration is repeated at each of the following time steps until the end of the simulation.

4 Stability boundary results

A parametric study was performed to obtain the stability boundary as Ea and Q were varied over a wide range. The stability boundary for each set of parameters was determined by varying K_r and finding the value below which the detonation becomes stable. γ and ν were kept constant at 1.2 and 0.5 respectively. A map of the stability boundary results can be found in Table 1. The period of oscillation tabulated in Table 1 is in terms of the induction time. The stability parameter, χ, is defined as the product of the activation energy and the ratio of the induction length to reaction length.

Table 1 shows that for high activation energy, low frequency pulsations are seen. For lower activation energies, where K_r at the stability boundary is higher (hence thinner reaction zones), and low heat release high frequency pulsations with a period of oscillation on the order of 2 induction times are seen. When activation energy is further lowered to $Ea = 1$, corresponding to even thinner reaction zones at the stability boundary, very high frequency pulsations with a period of oscillation of less than one induction time are seen. The results shown in Table 1 show four unique regimes of instability. Here, we focus on the novel regime of very high frequency pulsations. The other regimes have been described in detail in other works. [5, 7]

Table 1: The neutral stability boundary and the pulsating dynamics regimes.

E_a	Q	2.789	5.000	7.500	10.3875
1.0	Stability	$K_r = 15.93 \pm 0.01$	$K_r = 5.650 \pm 0.01$	$K_r = 2.889 \pm 0.001$	$K_r = 1.660 \pm 0.001$
	Boundary	$\chi = 12.8$	$\chi = 9.89$	$\chi = 8.82$	$\chi = 8.00$
	Regime[a]	VHF	VHF	VHF	VHF
	Period	0.67	0.57	0.78	0.72
5.0	Stability	$K_r = 2.680 \pm 0.002$	$K_r = 1.0384 \pm 0.001$	$K_r = 0.5385 \pm 0.0005$	$K_r = 0.360 \pm 0.001$
	Boundary	$\chi = 10.8$	$\chi = 9.09$	$\chi = 8.22$	$\chi = 8.7$
	Regime[a]	HF	HF	HF	T
	Period	2.0	1.7	1.6	1.4
					21
7.5	Stability	$K_r = 1.811 \pm 0.001$	$K_r = 0.6955 \pm 0.0005$	$K_r = 0.3515 \pm 0.0005$	$K_r = 0.2095 \pm 0.0005$
	Boundary	$\chi = 10.9$	$\chi = 9.13$	$\chi = 8.05$	$\chi = 7.57$
	Regime[a]	HF	T	T	T
	Period	2.0	1.7	1.6	1.5
			19	23	21
10.0	Stability	$K_r = 1.162 \pm 0.002$	$K_r = 0.4475 \pm 0.0005$	$K_r = 0.2415 \pm 0.0005$	$K_r = 0.1485 \pm 0.0005$
	Boundary	$\chi = 9.37$	$\chi = 7.84$	$\chi = 7.38$	$\chi = 7.15$
	Regime[a]	LF	LF	LF	LF
	Period	18	23	28	33

[a] Pulsating regimes: VHF=Very high frequency, HF=High frequency, T=Transition, LF=Low frequency

5 The high frequency regime

As highlighted by Table 1, high frequency pulsations with period of approximately 1.5 induction times are seen for moderate activation energy and low heat release close to the stability boundary. In this section, a simulation with parameters $E_a = 5$, $Q = 2.789$, $\gamma = 1.2$, $\nu = 0.5$ and $K_r = 3.200$ is examined in detail. The families of characteristics in the reaction zone structure are shown in Fig. 1.

Fig. 1 shows the detailed reaction zone dynamics in a frame of reference moving with velocity D_{CJ} in which the detonation wave is approximately stationary, on average. The C+ characteristics are represented by the solid lines travelling to the right. The particle paths are represented by the dashed lines moving to the left. Solid lines also mark the termination of the induction and reaction zones, respectively. Note that the apparent thickness of the detonation shock front is due to the trapping of the C+ characteristics in the numerical shock.

In Fig. 1, the pulsations of the lead shock front, the locus of the end of the induction zone and locus of the end of the reaction zone have the same period. The period of oscillation is well correlated by the sum of the times for a particle to move across the induction zone, and of a C+ characteristic to travel across the induction zone, as seen when following a particle path from *Point 1* to *Point 3*, then following the C+ characteristic from *Point 3* back to the shock at *Point 2*.

The apparent instability mechanism is consistent with that proposed by Toong and co-workers [2], and later studied by Matsuo an co-workers [9, 10]. Starting at $t = 780.6$, the hot particle or contact surface, originating from the shock at *Point 1* in Fig. 1, moves to the left across the induction zone and arrives at the reaction zone at *Point 3*. At this point, a strong compression wave is generated and moves toward the leading shock until it catches up at approximately $t = 783.6$. The arrival of this compression wave strengthens the lead shock front of the detonation, creates a new contact surface and triggers the start of the next cycle. The deceleration is due to the expansion waves coming from the reaction zone travelling along the C+ characteristics.

Fig. 1 shows that when the contact surface reaches the reaction zone at *Point 3*, the location of the start of the reaction zone is pulled toward the leading shock such that it is approximately parallel with the local C+ characteristics. Directly behind the induction zone the rate of heat release is highest. During this period the dynamics are such that the C+ characteristics are locally in phase with the onset of reactions. A mechanism likely to operate here is akin to the SWACER (Shock Wave Amplification through Coherent Energy Release) mechanism described by Yoshikawa. [11] For a short transient, the compression wave travelling along the C+ characteristic and the onset of the heat release appear to propagate along a common path, suggesting they are coherent and feedback, resulting in an amplification of the compression. Subsequent to this transient period, the paths diverge suggesting the compression wave and heat release rapidly decouple. The compression wave then emerges into the induction zone and hence subsequently propagates as an inert wave since there is no heat release in this zone.

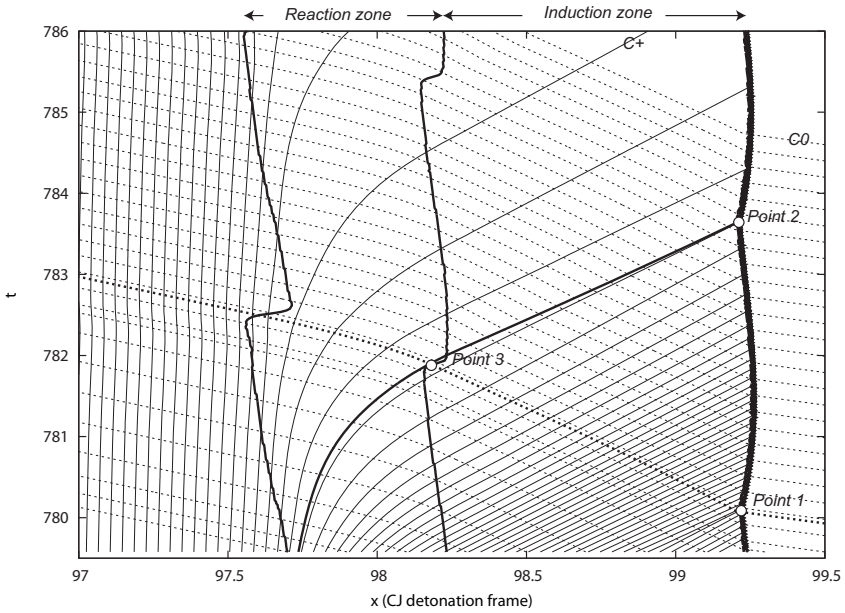

Figure 1: Families of characteristics for $E_a = 5$, $Q = 2.789$, $\gamma = 1.2$, $\nu = 0.5$, $K_r = 3.200$; solid lines moving to the right are the C+ characteristics; dashed lines moving to the left are the particle paths.

Increasing the value of K_r leads to a shorter reaction zone and thus higher rate of heat release along the path taken by the end of the induction zone. Due to this more rapid heat release, the amplification of the coherent compression wave is also faster, while for smaller values of K_r and thus longer reaction zones, the heat release occurs slowly and the compression waves do not amplify quickly enough for instabilities to arise. The role of the activation energy is to prescribe the timing of the onset of reaction. If the activation energy is too low, the onset of the reactions does not occur in phase with the generated compression wave, and the instability is suppressed. This mechanism thus provides a physical interpretation to how the χ parameter controls the onset of instability and the subsequent dynamics.

6 The very high frequency regime

Table 1 shows that for a very low activation energy, very high frequency oscillations with a period of less than one induction time are present. To the best of our knowledge, this regime was previously not identified. The very high frequency pulsations were studied using the parameters $E_a = 1$, $Q = 10.3875$, $\gamma = 1.2$, $\nu = 0.5$ and $K_r = 2.10$. The families of characteristics are shown in Fig. 2.

In Fig. 2, the C+ characteristics are represented by the solid lines moving to the right and the particle paths are represented by the thin dashed lines moving to the left. Two sample C- characteristics, originating from *Point 1* and *Point 2*, represented by the thin dotted lines are also shown.

As with the high frequency case, the shock and the induction zones are oscillating with the same period. However, in this case, the period is correlated instead by the time it takes for a C- to move across the induction zone from the shock, and the time it takes for a C+ to move across the induction zone toward the shock, as seen when following the C- from *Point 1* to *Point 3*, then following the C+ from *Point 3* back to the shock front at *Point 2*.

Starting at $t = 307.81$, an expansion wave originating from the shock front (*Point 1* on Fig. 2) is seen moving across the induction zone towards the reaction zone. This backward moving expansion wave originates from the interior right-moving shock that caught up to the lead shock at *Point 1*. Indeed, it is well known that a shock overtaking another shock gives rise to a contact discontinuity, as discussed above, and a reflected expansion wave of finite strength. [12]

When the expansion wave arrives at the reaction zone at approximately $t = 308.5$ (*Point 3* on Fig. 2), a compression wave is generated and travels toward the leading shock along the C+ characteristic, catching up to the shock

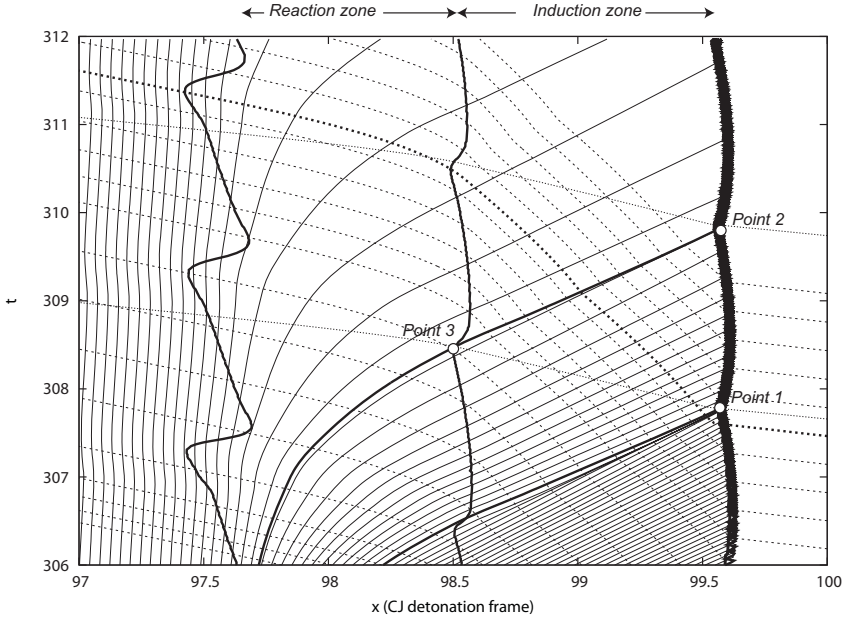

Figure 2: Family of characteristics for $E_a = 1$, $Q = 10.3875$, $\gamma = 1.2$, $\nu = 0.5$ and $K_r = 2.10$. Solid lines pointing to the right are the C+ characteristics, and the dashed lines moving to the left are the particle paths. Thin lines originating from *Point 1* and *Point 2* represent two sample C- characteristics.

front at roughly $t = 309.8$ (*Point 2* on Fig. 2). Note that this compression wave steepens up into a shock wave, as the C+ characteristics coalesce.

Fig. 2 indicates that the very high frequency pulsations are governed by the coupling between the expansion waves traveling along the C- and the compression waves traveling along the C+. The origin of these internal compression waves is likely to be due to the interaction of left-facing expansion waves with the reaction zone. When an expansion wave enters a region of lower acoustic impedance ρc, as is the case for a deflagration, a reflected train of compression waves is created. Indeed, the acoustic impedance in a perfect gas is:

$$\rho c = \rho\sqrt{\gamma p/\rho} = \sqrt{\gamma\rho p} \tag{7}$$

and both density and pressure decay in the reaction zone (flame) owing to the heat release. Hence, the acoustic impedance will decrease quickly in the reaction zone from that at the end of the induction zone. In separate numerical experiments, we have isolated this novel mechanism by triggering a strong expansion wave at the shock, and studied the interaction of the resulting left moving expansion wave with the reaction zone. The same result was observed of a reflected compression wave.

Note that in Fig. 2, the contact surface originating from *Point 1* arrives at the reaction zone at roughly the same time as the C- characteristic originating from *Point 2*. Since the C- and C0 characteristics trigger the same type of disturbances (reflected compressions), there are two mechanisms occurring simultaneously. In this case, the period of oscillation is half that of the high frequency oscillation studied above.

The coherence in the arrival of the C- and C0 at the reaction zone from lead shock disturbances occurring exactly one period of oscillation apart relies on the gas state in the induction layer conducive to this coupling. If t_-, t_+, and t_i denote the non-dimensional transit times for the C-, C+ and particle paths across the induction zone respectively, the condition for the coherence illustrated in Fig. 2 is that the arrival of the C- characteristic coincides with the arrival of the particle path disturbance originating at the previous cell cycle, i.e.,

$$2t_- + t_+ = t_i \tag{8}$$

which reduces to the requirement that the flow in the shock fixed frame must have a Mach number of 1/3. For $\gamma = 1.2$, this criterion is exactly satisfied when $Q = 9.7$, which is very close to the value considered above. With

lower heat release, the lead shock becomes weaker and the Mach number in the post shock gas increases rapidly (and tends to one for very weak heat release). We thus see that this mechanism is only promoted for large heat release.

7 Concluding remarks

In this work, the non-linear one-dimensional pulsating detonation instability was studied through a numerical investigation. In particular, the mechanisms governing very high frequency pulsations for an extremely low activation energy was examined in detail. The analysis of the dynamics between the induction and reaction zones were facilitated due to the simplicity of the two-step model. The mechanisms for instability were clarified through the reconstruction of the families of characteristics.

The very high frequency regime of instability studied in this work relies on two mechanisms. The first mechanism involves a coupling between the expansion waves travelling along the C- characteristics across the induction zone and the reflected compression waves moving along the C+ characteristics. The second mechanism involves a coupling between the contact surface and the compression waves moving along the same C+ characteristics as the former mechanism. The coherence of these two mechanisms enforce the very high frequency instability.

References

[1] W. Fickett and W. W. Wood, "Flow calculations for pulsating 1-dimensional detonations," *Physics of Fluids*, vol. 9, no. 5, pp. 903–916, 1966.

[2] J. B. McVey and T. Y. Toong, "Mechanism of instabilities of exothermic hypersonic blunt-body flows," *Combustion Science and Technology*, vol. 3, no. 2, pp. 63–76, 1971.

[3] J. J. Erpenbeck, "Stability of steady-state equilibrium detonations," *Physics of Fluids*, vol. 5, no. 5, pp. 604–614, 1962.

[4] H. I. Lee and D. S. Stewart, "Calculation of linear detonation instability - one-dimensional instability of plane detonation," *Journal of Fluid Mechanics*, vol. 216, pp. 103–132, 1990.

[5] M. Short and G. J. Sharpe, "Pulsating instability of detonations with a two-step chain-branching reaction model: theory and numerics," *Combustion Theory and Modelling*, vol. 7, no. 2, pp. 401–416, 2003.

[6] H. D. Ng, M. I. Radulescu, A. J. Higgins, N. Nikiforakis, and J. H. S. Lee, "Numerical investigation of the instability for one-dimensional chapman-jouguet detonations with chain-branching kinetics," *Combustion Theory and Modelling*, vol. 9, no. 3, pp. 385–401, 2005.

[7] C. Leung, M. I. Radulescu, and G. J. Sharpe, "Characteristics analysis of the one-dimensional pulsating dynamics of chain-branching detonations," *Physics of Fluids*, vol. 22, no. 12, p. 126101, 2010.

[8] J. J. Quirk, *Amrita A computational facility for CFD modelling*, 1998.

[9] A. Matsuo and T. Fujiwara, "Numerical investigation of oscillatory instability in shock-induced combustion around a blunt-body," *AIAA Journal*, vol. 31, no. 10, pp. 1835–1841, 1993.

[10] Y. Daimon and A. Matsuo, "Detailed features of one-dimensional detonations," *Physics of Fluids*, vol. 15, no. 1, pp. 112–122, 2003.

[11] N. Yoshikawa, "Coherent shock wave amplification in photochemical initiation of gaseous detonations," Ph.D. dissertation, McGill University, Montreal, 1980.

[12] G. V. Bull, L. B. Powell, and D. H. Henslaw, "The interaction of two similarly facing shock waves," *Journal of Aeronautical Science*, vol. 21, pp. 210–212, 1954.